

Effective working regions of the grating chip for planar-integrated magneto-optics trap

Chang-Jiang Huang(黄长江), Ling-Xiao Wang(王凌潇), Liang Chen(陈梁), Chuan-Feng Li(李传锋), Guang-Can Guo(郭光灿), Chang-Ling Zou(邹长铃), and Guo-Yong Xiang(项国勇)

Citation: Chin. Phys. B, 2025, 34 (**7**): 074211. DOI: 10.1088/1674-1056/adcb9c
http://cpb.iphy.ac.cn; http://iopscience.iop.org/cpb

What follows is a list of articles you may be interested in

Ultraviolet metalens and metalens array of focused vortex beams

Jinping Zhang(张金平), Yan Wang(王焱), Huan Yuan(袁欢), Zehao Wang(王泽豪), Yang Deng(邓阳),Chengzhi Huang(黄承志), Jiagui Wu(吴加贵), and Junbo Yang(杨俊波)

Chin. Phys. B, 2023, 32 (**6**): 064206. DOI: 10.1088/1674-1056/ac9d87

Observation of V-type electromagnetically induced transparency and optical switch in cold Cs atoms by using nanofiber optical lattice

Xiateng Qin(秦夏腾), Yuan Jiang(蒋源), Weixin Ma(马伟鑫), Zhonghua Ji(姬中华),Wenxin Peng(彭文鑫), and Yanting Zhao(赵延霆)

Chin. Phys. B, 2022, 31 (**6**): 064216. DOI: 10.1088/1674-1056/ac685a

Sensitivity enhancement of micro-optical gyro with photonic crystal

Liu Yang(杨柳), Shuhua Zhao(赵舒华), Jingtong Geng(耿靖童), Bing Xue(薛冰), and Yonggang Zhang(张勇刚)

Chin. Phys. B, 2021, 30 (**4**): 044208. DOI: 10.1088/1674-1056/abe3f3

Improve the performance of interferometer with ultra-cold atoms

Xiangyu Dong(董翔宇), Shengjie Jin(金圣杰), Hongmian Shui(税鸿冕), Peng Peng(彭鹏), and Xiaoji Zhou(周小计)

Chin. Phys. B, 2021, 30 (**1**): 014210. DOI: 10.1088/1674-1056/abcf33

Linear optical approach to supersymmetric dynamics

Yong-Tao Zhan(詹颙涛), Xiao-Ye Xu(许小冶), Qin-Qin Wang(王琴琴), Wei-Wei Pan(潘维韦), Munsif Jan, Fu-Ming Chang(常弗鸣), Kai Sun(孙凯), Jin-Shi Xu(许金时), Yong-Jian Han(韩永建), Chuan-Feng Li(李传锋), Guang-Can Guo(郭光灿)

Chin. Phys. B, 2020, 29 (**1**): 014209. DOI: 10.1088/1674-1056/ab5efe

---

Effective working regions of the grating chip for planar-integrated magneto-optics trap

Chang-Jiang Huang(黄长江)[1,2,†], Ling-Xiao Wang(王凌潇)[1,2,†], Liang Chen(陈梁)[1,2], Chuan-Feng Li(李传锋)[1,2,3], Guang-Can Guo(郭光灿)[1,2,3], Chang-Ling Zou(邹长铃)[1,2,3,‡], and Guo-Yong Xiang(项国勇)[1,2,3,§]

[1] *Laboratory of Quantum Information, University of Science and Technology of China, Hefei* 230026, *China*
[2] *CAS Center for Excellence in Quantum Information and Quantum Physics, University of Science and Technology of China, Hefei* 230026, *China*
[3] *Hefei National Laboratory, University of Science and Technology of China, Hefei* 230088, *China*

(Received 4 March 2025; revised manuscript received 10 April 2025; accepted manuscript online 11 April 2025)

We experimentally investigate the effective working regions of a planar-integrated magneto-optical trap (MOT). By scanning a blocking point in the incident laser beam, we identify four effective working regions of the laser beam contributing to MOT: a central region corresponding to the downward incident beam and three regions associated with the upward diffracted beams. The latter three regions are the effective regions of the grating chip. It is demonstrated that only three 3.5 mm radius grating regions can produce a MOT that is capable of trapping 10^5 atoms with a temperature below 150 μK, retaining over 60% of atoms compared to a complete grating chip. This finding suggests that more than 60% of the grating chip area can be saved for other on-chip components, such as metasurfaces and nanophotonic devices, without significantly compromising MOT performance, paving the way for more compact and versatile atom–photon interfaces.

Keywords: cold atoms, grating chip, magneto-optical trap (MOT)

PACS: 42.79.Dj, 42.62.–b, 37.10.–x, 37.10.Gh

DOI: 10.1088/1674-1056/adcb9c **CSTR:** 32038.14.CPB.adcb9c

1. Introduction

Cold atoms are widely used in the fields of quantum communication,[1–6] quantum computing,[7–11] and quantum precision measurement.[12–15] One of the most important experimental platforms in atomic physics is the magneto-optical trap (MOT), which is typically composed of complex optical components and bulky magnetic field coils.[16] Over the past decade, many research groups have carried out work on minimizing the MOT system. The incident laser is reduced to only one beam with a pyramidal retroreflector,[17–20] which is further replaced with a completely flat grating chip.[21–26] Also, the original bulky anti-Helmholtz coils are replaced by a planar coil chip in recent works.[27–29] With these efforts, the traditional MOT can finally be simplified to a planar-integrated MOT. These miniaturized MOT systems based on chips offer several key advantages. First, they drastically reduce the size, weight and power requirements compared to traditional MOT setups, making them more portable and easier to deploy in field applications.[30–36] Second, the planar geometry is inherently more scalable, allowing the integration with other on-chip optical devices[37–41] and even allowing the realization of arrays of MOTs on a single chip for parallel operation. Third, the planar chip-based platform facilitates integration with other quantum devices and technologies, providing a promising hybrid quantum platform to incorporate atoms with other systems.[42–46]

However, current planar grating MOT designs have some drawbacks that limit their performance and flexibility. First, the grating requires a large incident beam, typically over 10 mm in diameter, to ensure sufficient laser intensity in the trapping region. As a result, the laser power needed often exceeds 50 mW, which is challenging for power-limited applications. Second, the grating chip is completely covered with the diffractive structure, leaving no room for incorporating other components on the same chip that could enable novel atom-photon interfaces. The incorporation of metasurfaces, waveguides, microresonators, and functional optical switches and modulators onto the MOT chip has the potential to unlock new possibilities in quantum memories, nanoscale sensing, and information processing. However, such multi-functional integration remains infeasible with the current fully-committed grating design. To address these limitations, it is crucial to identify the effective working regions of the grating chip that contribute to atom trapping. By doing so, we can develop power-efficient and area-efficient planar-integrated MOTs.

In this work, we experimentally investigate the effective working regions of the incident laser beam and the grating chip that contribute to the MOT operation. Our experiments reveal that the grating chip has three effective regions, while the remaining areas can be removed without destroying the MOT. In

†These authors contributed equally to this work.
‡Corresponding author. E-mail: clzou321@ustc.edu.cn
§Corresponding author. E-mail: gyxiang@ustc.edu.cn

© 2025 Chinese Physical Society and IOP Publishing Ltd. All rights, including for text and data mining, AI training, and similar technologies, are reserved.

the case that the central circular region with a radius of 0.5 mm is obscured and only three central symmetrical through-light regions with a radius of 3.5 mm are retained, the grating chip can still successfully trap around 10^5 rubidium atoms and cool them to a temperature below 150 μK. The useless region of the grating chip can be excised, leaving valuable space for introducing more functionalities to the compact MOT system, or integrating nanophotonic devices for photonic–atomic hybrid chip systems.

2. Planar-integrated MOT

The planar-integrated MOT configuration in this work combines a grating chip and a planar coil chip.[27] As illustrated in Fig. 1(a), the planar-integrated MOT relies on the pyramid-like optical beams for laser cooling. The incident beam is transformed into three diffraction beams with designed directions and polarizations by the planar grating chip, which overlap above the chip. By adjusting the grating period and duty cycle of the etched gratings, we can control the intensity and diffraction angle of the three diffraction beams and balance the radiation pressure experienced by the atoms in the overlapping regions. The grating and the planar coil chips, as shown in Figs. 1(b) and 1(c), are identical to those used in our previous work.[27] The grating chip is divided into three uniform grating regions with their directions different by 120°. The measured diffraction angle θ with respect to the grating plane, as depicted in Fig. 1(a), is 42.4°. The planar coil chip consists of two coaxial coils with different radii, numbers of turns, and opposite currents. By adjusting these parameters, we can tune the operating point, i.e., the zero field point of a quadratic magnetic field, of the coil chip.

In our experiment, external-cavity diode lasers are tuned to the 780 nm to match the D2 line transitions of Rubidium atoms (^{87}Rb). The cooling laser is tuned to the $^5S_{1/2}(F=2)$ to $^5P_{3/2}(F=3)$ cycling transition with a detuning of about −9 MHz, while the repump laser is tuned to the $^5S_{1/2}(F=1)$ to $^5P_{3/2}(F=2)$ transition. The incident beam, composed of these two laser beams, has a diameter of about 3.0 cm and an optical intensity of 20 mW/cm^2 for the cooling laser and 2 mW/cm^2 for the repump laser. The zero point of the magnetic field in the central axis is set to 6.3 mm above the surface of the coil chip with a current of $I = 2$ A applied to the chip. As shown in Fig. 1(d), both chips are placed outside the glass vacuum cell, and the coil chip is aligned to the grating chip to match the working points of the two chips. The effective laser cooling process takes place in a relatively large volume within the vacuum chamber, making it challenging to directly predict the effective working regions of the grating chip. Nonetheless, we can simplify the problem by focusing on the specific locations that contribute to the working point of the MOT. By considering the zero point of the magnetic field, the influence of the cell wall thickness (2 mm), and the diffraction angle, we can identify three essential points (regions) on the grating chip, each approximately 3.6 mm from the center. Due to the symmetry of the grating chip, these points lie on the mirror-symmetric axis of each grating sector and are separated by 120° from each other.

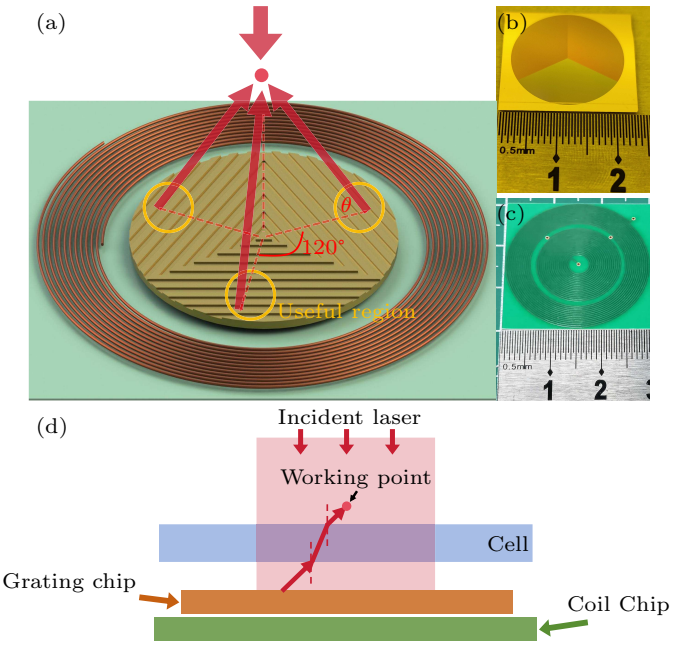


Fig. 1. (a) Schematic of the planar-integrated magneto-optical trap (MOT). (b) Photograph of the grating chip. (c) Photograph of the planar coil chip. (d) Due to the presence of the glass cell, the diffracted light field experiences refraction, leading to an offset of the central position of the effective region.

In the following, we execute experiments to investigate the effective working regions of the grating chip and verify the above predictions. Since the optical laser, not the grating itself, directly contributes to the laser cooling and, consequently, the MOT, we can characterize the effective working regions of the input laser beam. By first identifying the regions of the incident optical beam that contribute to the MOT and identifying the critical optical paths and their corresponding regions, we can then fabricate masks to block the unnecessary regions of the optical laser beam. This approach allows us to systematically block the unnecessary regions of the grating chip, optimizing the MOT's performance and efficiency while saving space on the grating chip.

3. Effective working regions of incident light

To determine the critical optical paths and their corresponding regions essential for the MOT's operation, we systematically block specific regions of the incident laser beam and measure the resulting atom number in the MOT. As depicted in Fig. 2(a), we introduce a 0.5 mm thick circular glass window and affix a round black cardboard with 0.5 mm radius as the blocking point to the planar-integrated MOT sys-

tem. The glass window with the blocking point is driven by a two-dimensional stepper motor, allowing it to perform a two-dimensional scan in the directions shown in Fig. 2(b).

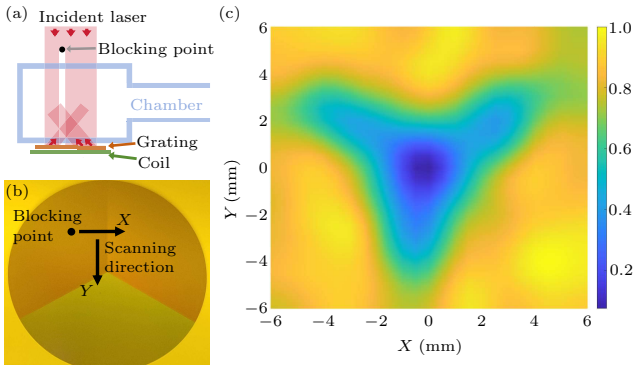


Fig. 2. (a) Schematic of the blocking point approach to probe the effective working region of the incident laser beam. (b) The blocking point undergoes two-dimensional motion along the X and Y directions. (c) Results of the position scanning of the blocking point, showing the normalized atom number in the MOT as a function of the blocking point position.

By adjusting the position of the window, we can control the region where the incident light is obstructed by the blocking point and measure the atom number under this state. A lower atom number indicates greater significance in terms of blocking specific regions within the incident light field. Through program-controlled scanning of blocked locations, we establish a correlation between atom number in our obtained MOT and the occlusion positions, as illustrated in Fig. 2(c). The coordinates represent the relative positions from the center of the incident laser. The scanning step length is set as 0.5 mm, and the blocking point moves along the X and Y directions, covering a total area of 12 mm $\times$ 12 mm. For better data visualization, the atom counts data are normalized to the maximum value and smoothed to ensure clarity in our scan results.

From Fig. 2(c), it becomes evident that there exist four effective regions within the incident light field, which correspond to four beams forming the optical field of the planar-integrated MOT: one central region aligns with vertically downward illumination, while three external regions correspond to diffracted upward beams. Meanwhile, the distances between the three effective external regions (about 3 mm) and the center agree with the theoretical predictions.

Based on the results of the obscuration scan, we further investigate the effects of simultaneously blocking the light fields in these ineffective regions on the performance of the MOT. We fabricate a blocking plate with four circular holes of equal radius, as depicted in Fig. 3(a), ensuring that only the light fields within the effective regions remained unblocked and reached the grating chip. This blocking plate is fabricated using 3D printing technology, as displayed in Fig. 3(b), enabling us to easily create samples with varying circular hole radii.

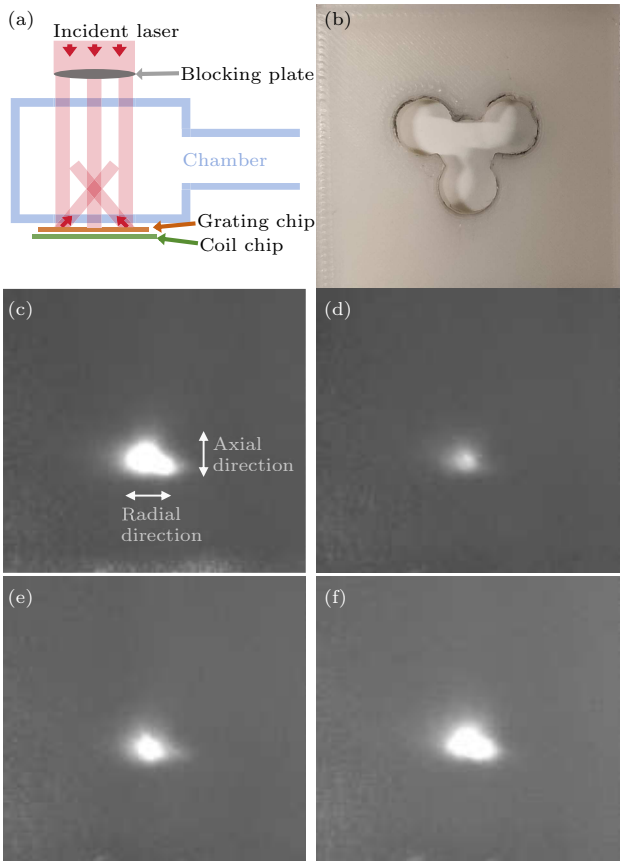


Fig. 3. (a) The schematic of the blocking of the incident light field. (b) The real 3D-printed blocking plate. (c)–(f) Images of the atom clouds under different experimental conditions: with no blocking plate and with blocking plates having holes of varying radii of 2.5 mm, 3.5 mm, 4.5 mm.

Subsequently, we capture images of the MOT fluorescence under different experimental conditions. As presented in Figs. 3(c)–3(f), the images are taken for blocking plates with varying radii of ∞ (no blocking plate), 2.5 mm, 3.5 mm, and 4.5 mm, respectively. Here, the camera is set at an exposure time of 5 ms. It can be observed that as the aperture size decreases, fewer atoms can be trapped within the MOT, confirming that only the four regions contribute to the formation of the MOT. The measurement results are shown in Table 1.

Table 1. The temperature and atom number with different hole radii of the blocking plates.

Radius of holes (mm)	2.5	3.5	4.5
Radial temperature (μK)	–	148 ± 15	114 ± 15
Axial temperature (μK)	–	126 ± 9	112 ± 6
Atom number (10^5)	0.32 ± 0.06	0.89 ± 0.09	1.5 ± 0.1

4. Effective working regions of grating chip

Upon characterizing the effective region of the light field, we proceed to investigate the effective region of the grating chip by directly covering its surface with the blocking plate. Contrary to the previous setup, the blocking plate is placed between the grating chip and the vacuum chamber, as shown in Fig. 4(a). The effective region of the incident light includes

the center region, where a downward-directed light field is required to provide trapping force. However, the grating chip actually does not require the central region. We first only block the center of the grating chip, using two different sizes of the blocking point: circles with radii approximately measuring 0.5 mm and 1 mm, as depicted in the center of Fig. 4(b). In both cases, a MOT can be formed and the atoms are polarization gradient cooled (PGC)[47] in 0.5 ms with a detuning −40 MHz from resonance. We then measure the temperature and number of the atoms.

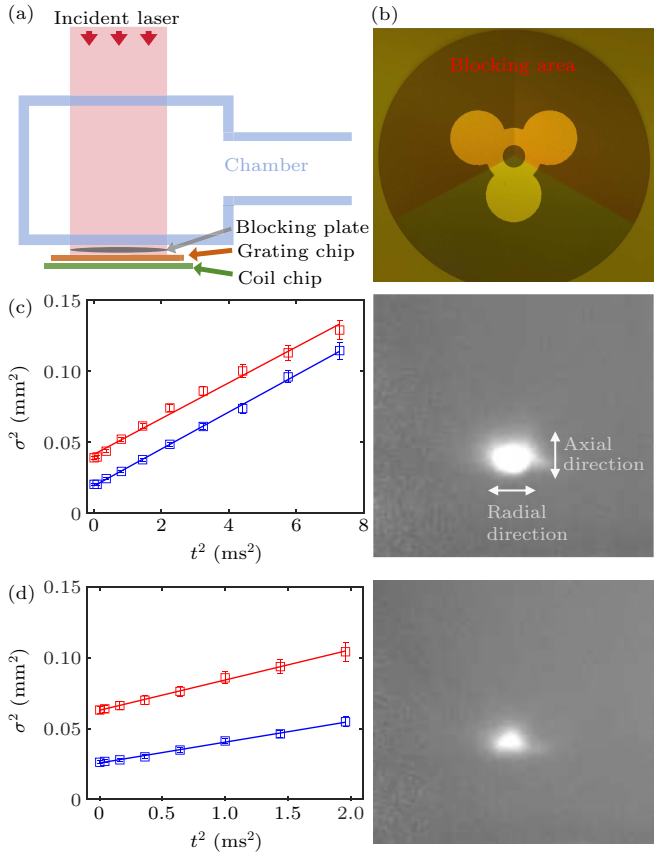


Fig. 4. (a) Schematic of the blocking of the grating chip. (b) Schematic of the blocking region of the grating chip. (c) The experimental results of the atom cloud sizes against free expansion time with a blocking point of 0.5 mm radius and fluorescence from trapped atoms. (d) The experimental results of the atom cloud sizes against free expansion time with a blocking point of 1 mm radius and fluorescence from trapped atoms.

Figures 4(c) and 4(d) show the fitted squared $1/\mathrm{e}$ radii of the atom cloud in the radial (red points) and axial (blue points) directions versus the squared free expansion time t for blocking points of 0.5 mm and 1 mm radius, respectively. The two lines are the fits of $\sigma^2 = \sigma_0^2 + k_\mathrm{B}Tt^2/m$ to the data, where σ is the $1/\mathrm{e}$ radius of the atom cloud in the radial (red line) or axial (blue line) direction, k_B is the Boltzmann constant, T is the temperature, and m is the mass of an ^{87}Rb atom. For a blocking point of 0.5 mm radius, the temperature in radial and axial directions can reach 121 ± 14 μK and 125 ± 6 μK, respectively. The atom number is $N = (1.45 \pm 0.27) \times 10^5$. However, when the radius of the blocking point increases to 1 mm, the temperatures in radial and axial directions increase to 205 ± 14 μK and 141 ± 13 μK, with an atom number of $N = (7.7 \pm 1.8) \times 10^4$. As a comparison, when there is no blocking point at all, the temperatures are 100 ± 23 μK and 132 ± 5 μK, with an atom number of $N = (1.65 \pm 0.3) \times 10^5$. It can be seen that the blocking point of 0.5 mm radius has a limited effect on the atomic temperature and number, but a larger blocking area in the center of the grating chip can affect the temperature and atom number obviously. The increase in the radius of the central obstruction will block three surrounding effective regions, thereby compromising the completeness of the optical fields that constitute the magneto-optical trap. Photos of cold atoms in the MOT are also shown in Figs. 4(c) and 4(d) with 5 ms exposure time. Based on the results with the center of the grating chip blocked, we further combined it with the effective region of the light field. As displayed in Fig. 4(b), the center and periphery of the grating chip are both blocked, which can be further hollowed out or etched and combined with additional nanophotonic circuits. The central blocking region's radius is 0.5 mm and we use three kinds of black cardboard to block the peripheral region of the chip and fine-tune the position of the cardboard to make atoms captured by the grating chip reach the best state. The holes on the cardboard have varying radii of 2.5 mm, 3.5 mm, and 4.5 mm, corresponding to the previous blocking plates that block the incident light. The distance between the center of the outer three holes of the occlusion and the center of the grating is 3.6 mm.

The measurement results are shown in Table 2. When using black cardboard with 2.5 mm radius holes, the atom number is too small. Thus we cannot measure the temperature properly by the method of absorption imaging, only the atom number is exhibited. It can be seen that the atom number decreases when the hole radius of the cardboard decreases, but the temperature is basically similar. With the central region of the grating chip obscured by a circle with 0.5 mm radius and only three symmetrical regions with 3.5 mm radius retained, the temperature in radial and axial directions can reach 149 ± 9 μK and 107 ± 14 μK, with an atom number of $N = (9.9 \pm 1.2) \times 10^4$. This demonstrates that the grating chip can still capture a certain number of cold atoms even when over 60% of the total area is obscured. When the radii of the holes increase to 4.5 mm, the atomic number and atomic temperature can basically return to the situation without shelter, indicating that the obscured part of the grating chip hardly participates in the formation of MOT.

Table 2. The temperature and atom number with different hole radii of the cardboard.

Radius of holes (mm)	2.5	3.5	4.5
Radial temperature (μK)	–	149 ± 9	139 ± 15
Axial temperature (μK)	–	107 ± 14	129 ± 11
Atom number (10^5)	0.27 ± 0.2	0.99 ± 0.12	1.62 ± 0.05

5. Conclusion

In conclusion, the effective working regions of the incident laser and the grating chip are experimentally investigated for a planar-integrated MOT system. Three regions of the grating chip are identified through two different approaches, i.e., blocking the incident light and directly blocking the grating chip. It is verified that only three symmetrical regions of 3.5 mm radius are necessary for the MOT, which can trap 10^5 atoms at a temperature lower than 150 μK. This finding suggests that more than 60% of the grating chip area can be saved. By leveraging the saved space on the grating chip, we can explore the development of compact and versatile quantum devices that combine the advantages of cold atoms and nanophotonics. Additionally, the investigation of advanced grating designs, such as metasurfaces with tailored phase and polarization control, could further enhance the performance and functionality of the planar-integrated MOT.

Acknowledgments

Project supported by the National Key R&D Program of China (Grant Nos. 2021YFA1402004 and 2021YFF0603701) and the National Natural Science Foundation of China (Grant Nos. 12134014, U21A20433, U21A6006, and 92265108). This work was also supported by the Fundamental Research Funds for the Central Universities and USTC Research Funds of the Double First-Class Initiative. The numerical calculations in this paper have been done on the supercomputing system in the Supercomputing Center of the University of Science and Technology of China. This work was partially carried out at the USTC Center for Micro and Nanoscale Research and Fabrication.

References

[1] Duan L M, Lukin M D, Cirac J I and Zoller P 2001 *Nature* **414** 413
[2] Matsukevich D and Kuzmich A 2004 *Science* **306** 663
[3] Chou C W, Laurat J, Deng H, Choi K S, De Riedmatten H, Felinto D and Kimble H J 2007 *Science* **316** 1316
[4] Yuan Z S, Chen Y A, Zhao B, Chen S, Schmiedmayer J and Pan J W 2008 *Nature* **454** 1098
[5] Radnaev A, Dudin Y, Zhao R, Jen H, Jenkins S, Kuzmich A and Kennedy T 2010 *Nat. Phys.* **6** 894
[6] Wang X, Wang J, Ren Z, Wen R, Zou C L, Siviloglou G A and Chen J 2022 *Phys. Rev. Lett.* **128** 083605
[7] Saffman M, Walker T G and Mølmer K 2010 *Rev. Mod. Phys.* **82** 2313
[8] Endres M, Bernien H, Keesling A, Levine H, Anschuetz E R, Krajenbrink C, Senko V, Vuletic V, Greiner M and Lukin M D 2016 *Science* **354** 1024
[9] Barredo D, De Léséleuc S, Lienhard V, Lahaye T and Browaeys A 2016 *Science* **354** 1021
[10] Saffman M 2016 *J. Phys. B: At. Mol. Opt. Phys.* **49** 202001
[11] Bluvstein D, Evered S J, Geim A A, Li S H, Zhou H, Manovitz T, Ebadi M, Cain M, Kalinowski M, Hangleiter D, *et al.* 2024 *Nature* **626** 58
[12] Cronin A D, Schmiedmayer J and Pritchard D E 2009 *Rev. Mod. Phys.* **81** 1051
[13] Wu X, Pagel Z, Malek B S, Nguyen T H, Zi F, Scheirer D S and Müller H 2019 *Sci. Adv.* **5** eaax0800
[14] Asenbaum P, Overstreet C, Kim M, Curti J and Kasevich M A 2020 *Phys. Rev. Lett.* **125** 191101
[15] Ludlow A D, Boyd M M, Ye J, Peik E and Schmidt P O 2015 *Rev. Mod. Phys.* **87** 637
[16] Raab E L, Prentiss M, Cable A, Chu S and Pritchard D E 1987 *Phys. Rev. Lett.* **59** 2631
[17] Lee K, Kim J, Noh H and Jhe W 1996 *Opt. Lett.* **21** 1177
[18] Vangeleyn M, Griffin P F, Riis E and Arnold A S 2009 *Opt. Express* **17** 13601
[19] Pollock S, Cotter J, Laliotis A and Hinds E 2009 *Opt. Express* **17** 14109
[20] Pollock S, Cotter J, Laliotis A, Ramirez-Martinez F and Hinds E 2011 *New J. Phys.* **13** 043029
[21] Vangeleyn M, Griffin P F, Riis E and Arnold A S 2010 *Opt. Lett.* **35** 3453
[22] Nshii C, Vangeleyn M, Cotter J P, Griffin P F, Hinds E, Ironside C N, See P, Sinclair A, Riis E and Arnold A S 2013 *Nat. Nanotech.* **8** 321
[23] McGilligan J P, Griffin P F, Riis E and Arnold A S 2015 *Opt. Express* **23** 8948
[24] Cotter J, McGilligan J, Griffin P, Rabey I, Docherty K, Riis E, Arnold A and Hinds E 2016 *Appl. Phys. B* **122** 1
[25] Lee J, Ding R, Christensen J, Rosenthal R R, Ison A, Gillund D P, Bossert D, Fuerschbach K H, Kindel W, Finnegan P S, *et al.* 2022 *Nat. Commun.* **13** 5131
[26] Duan J, Liu X, Zhou Y, Xu X B, Chen L, Zou C L, Zhu Z, Yu Z, Ru N and Qu J 2022 *Opt. Commun.* **513** 128087
[27] Chen L, Huang C J, Xu X B, Zhang Y C, Ma D Q, Lu Z T, Wang Z B, Chen G J, Zhang J Z, Tang H X, *et al.* 2022 *Phys. Rev. Appl.* **17** 034031
[28] Yu Z, Zhu Y, Yao M, Qi F, Chen L, Zou C L, Duan J and Liu X 2024 *Opt. Express* **32** 8919
[29] Huang C J, Liu H C, Chen L, Li C F, Guo G C, Zou C L and Xiang G Y 2025 *Chin. Phys. Lett.* **42** 034203
[30] Vetsch E, Reitz D, Sagué G, Schmidt R, Dawkins S and Rauschenbeutel A 2010 *Phys. Rev. Lett.* **104** 203603
[31] Dang H, Maloof A C and Romalis M V 2010 *Appl. Phys. Lett.* **97** 102508
[32] Ritsch H, Domokos P, Brennecke F and Esslinger T 2013 *Rev. Mod. Phys.* **85** 553
[33] Goldman N, Juzeliūnas G, Öhberg P and Spielman I B 2014 *Rep. Prog. Phys.* **77** 126401
[34] Yang P, Xia X, He H, Li S, Han X, Zhang P, Li G, Xu J, Yang Y, *et al.* 2019 *Phys. Rev. Lett.* **123** 233604
[35] Hsu T W, Zhu W, Thiele T, Brown M O, Papp S B, Agrawal A and Regal C A 2022 *PRX Quantum* **3** 030316
[36] Chen G J, Wang J J, Wang Z B, Zhao D, Zhang Y L, Liu A P, Dong C H, Huang K, Guo G C and Zou C L 2024 *Opt. Express* **32** 39039
[37] Le Kien F, Gupta S D, Balykin V and Hakuta K 2005 *Phys. Rev. A* **72** 032509
[38] Fujiwara M, Toubaru K, Noda T, Zhao H Q and Takeuchi S 2011 *Nano Lett.* **11** 4362
[39] Yalla R, Le Kien F, Morinaga M and Hakuta K 2012 *Phys. Rev. Lett.* **109** 063602
[40] Barker D S, Norrgard E B, Klimov N N, Fedchak J A, Scherschligt J and Eckel S 2019 *Phys. Rev. Appl.* **11** 064023
[41] Blumenthal D J, Isichenko A and Chauhan N 2024 *Optica Quantum* **2** 444
[42] Zhuang W, Zhao Y, Wang S, Fang Z, Fang F and Li T 2021 *Chin. Opt. Lett.* **19** 030201
[43] Amico L, Anderson D, Boshier M, Brantut J P, Kwek L C, Minguzzi A and von Klitzing W 2022 *Rev. Mod. Phys.* **94** 041001
[44] Ropp C, Zhu W, Yulaev A, Westly D, Simelgor G, Rakholia A, Lunden W, Sheredy D, Boyd M M, Papp S, *et al.* 2023 *Light Sci. Appl.* **12** 83
[45] Isichenko A, Chauhan N, Bose D, Wang J, Kunz P D and Blumenthal D J 2023 *Nat. Commun.* **14** 3080
[46] Yu M, Cheng R, Reimer C, He L, Luke K, Puma E, Shao L, Shams-Ansari A, Ren X, Grant H R, *et al.* 2023 *Nat. Photon.* **17** 666
[47] Dalibard J and Cohen-Tannoudji C 1989 *J. Opt. Soc. Am. B* **6** 2023